PAPER

Check for updates

Dual-action prevention of adherent and non-adherent biofouling *via* slippery, nitric oxide-releasing nanoemulsion-infused porous surfaces

Grace H. Nguyen, Aasma Sapkota and Elizabeth J. Brisbois [ID] *

Contemporary clinical problems, such as medical device failure due to onset infection and thrombosis, pose a significant threat to the care and treatment of critical patients. While infection is typically treated with broad-spectrum antibiotics, and thrombosis is treated with systemic administration of anticoagulants, these options are less favorable because of the escalation of antibiotic resistance and adverse anticoagulation effects such as excessive bleeding and platelet consumption. Alternative strategies must be considered to address these issues before the current strategies become ineffective and cause irreversible damage. One such strategy is the combination of a bioactive therapeutic, nitric oxide (NO), with a passive anti-fouling technique, slippery nanoemulsion-infused porous surfaces (SNIPS). Loading the NO donor *S*-nitrosoglutathione (GSNO) into the aqueous phase of an oil-based nanoemulsion (NE) and infusing the NE into the porous expanded polytetrafluoroethylene (ePTFE) fabricated a dual-action material as an alternative to current devices, such as indwelling silicone rubber catheters, that physically prevented and repelled fouling agents from adhering to the surface while also releasing a bioactive gaseous molecule to kill bacteria. The ePTFE infused with the GSNO-NE was able to maintain slippery behavior and physiological levels of NO for 24 h. The combination material remained cytocompatible with a relative cell viability >70% while significantly reducing gram-positive *Staphylococcus aureus* (*S. aureus*) and gram-negative *Escherichia coli* (*E. coli*) adhesion. The material also did not elicit any hemolytic effects when exposed to dilute whole blood. The ePTFE infused with the GSNO-NE demonstrated promising results with potential to be applied in biomedical applications.

1. Introduction

Clinical complications in a healthcare setting, such as infection and venous thromboembolism, attribute to some of the leading causes of death within a hospital, with a 3.2% incidence rate for infection[1] and more than 30% incidence rate for venous thromboembolism.[2] Indwelling medical devices are particularly susceptible to device failure due to infection, thrombosis, or obstruction. Over 2 000 000 patients contract a hospital-acquired infection (HAI) annually with 50–70% stemming from implanted medical devices.[3] Patients with indwelling blood-contacting devices develop thrombus that prevent the device from functioning properly at an incidence rate of up to 6.4% annually.[4–7] While healthcare settings are equipped to treat and manage these complications through current gold standard treatment options like broad-spectrum antibiotics, systemic administration of anticoagulants, or device removal and replacement, it is a costly and resource-consuming task to

School of Chemical, Materials, and Biomedical Engineering, University of Georgia, Athens, GA, 30602, USA. E-mail: ejbrisbois@uga.edu; Tel: +706-542-1243

undertake. Infections alone can cost a hospital between $28.4 billion to $45 billion annually for treatment and extended hospital stays.[8,9]

Although antibiotics have been considered the gold standard for the treatment of bacterial infections and systemic administration of anticoagulants to treat and prevent blood clotting for decades, recent research moves away from antibiotic and systemic anticoagulant treatment to prevent further antibiotic resistance among common bacterial pathogens[10–12] and adverse effects associated with anticoagulants, such as excessive bleeding or the premature consumption of platelets.[13–15] To address the prevalent problem of these complications, nitric oxide (NO), an endogenously-produced gasotransmitter with inherent antibacterial and anti-platelet functionalities, has been synthetically incorporated *via* NO donors into several medically relevant polymers, such as silicone rubbers and polyurethanes, rendering them effectively more antibacterial and antithrombotic compared to their non-NO-releasing controls.[16–22] A class of NO donors called *S*-nitrosothiols (RSNOs) has been developed in the recent decades for the facile incorporation into these polymers; RSNOs can be catalyzed by thermal exposure, photocatalysis,

and metal ion interaction to release NO. Typically, these RSNOs, like *S*-nitrosoglutathione (GSNO) or *S*-nitroso-*N*-acetyl-penicillamine (SNAP), can be incorporated into polymers through simple blending[20] or impregnation techniques.[23] However, incorporation into fluorinated polymers remains a challenge due to the highly hydrophobic and chemically inert nature of these polymers.[24–27] Despite this challenge, GSNO is a highly water-soluble RSNO and can be especially effective for its antibacterial capacity in shorter-term applications due to the primary structure of the molecule.[28–30] Although GSNO tends to be more easily incorporated into hydrophilic mediums,[31,32] it has been integrated into more hydrophobic polymers, such as poly(vinyl chloride) (PVC)[18] and a polycarbonate-based silicone polyurethane, Chronosil.[21] However, to date, GSNO has not been incorporated into a fluorinated polymer. Additionally, while NO has excellent antibacterial and anti-platelet activity, it alone struggles to prevent biofouling on biomaterial surfaces due to bacterial, platelet, or protein adhesion.

Surface modifications, such as artificially roughened or modified wettability surfaces, have been widely researched and developed as techniques to combat infection, thrombosis, and biofouling.[33–38] Slippery surfaces have been at the forefront of this research, capitalizing on inherent polymer capabilities, such as porosity, to swell with certain solvents. Taking inspiration from the *Nepethes* pitcher plant, the Aizenburg group developed slippery liquid-infused porous surfaces (SLIPS).[39] The fundamental slippery property of SLIPS lies in the swelled lubricant reservoir within the polymer matrix; this reservoir serves as a source to replenish the surface lubricant that is lost due to external abrasion or dynamic fluid flow.[40,41] These SLIPS substrates can then demonstrate excellent wettability and slippery behavior, easily able to exhibit reduction in bacterial adhesion or blood component fouling.[17,39,42]

However, research has taken it a step further with the development of slippery nanoemulsion (NE)-infused porous surfaces (SNIPS),[43] a NE-based derivative of SLIPS. By definition, a NE is a solution of immiscible fluids, typically water and oil, that have been forcibly combined to form nano-sized droplets dispersed within a bulk continuous phase (*e.g.*, a water-in-oil (w/o) NE consists of oil as the continuous phase and water as the dispersed nano-droplets).[44,45] These SNIPS surfaces employ a w/o NE that is capable of loading water-soluble agents into the aqueous phase to combine a bioactive agent with a passive slippery surface.[43] By masking the aqueous phase in a continuous hydrophobic oil phase as aqueous nano-droplets, water-soluble drugs can be incorporated into hydrophobic substrates that would not otherwise be capable of swelling aqueous media. The combination of active and passive strategies will allow for the dual-action mechanism to prevent infection and thrombosis.

In this present work, a combination of a w/o NE and the water-soluble GSNO was infused into a porous expanded polytetrafluoroethylene (ePTFE) to fabricate a dual-action slippery and NO-releasing substrate capable of repelling adherent foulants as well as preventing planktonic foulants from con-

tacting the surface (Fig. 1). Here, two concentrations of GSNO were dissolved in 10 mM PBS with 100 μM EDTA and used as the aqueous phase of the NE. The NE was then fabricated by slowly introducing the oil phase to the aqueous phase under low-energy magnetic stirring followed by high-energy sonication. The GSNO-NEs were then infused into the ePTFE, and the surface characteristics were evaluated *via* sliding angle measurement and NE stability over 24 h. The NO release profile was assessed over 24 h, and the biocompatibility, namely cytocompatibility and hemocompatibility, were evaluated using NIH 3T3 mouse fibroblast cells, human umbilical vein endothelial cells (HUVEC), and diluted porcine whole blood, respectively. The antibacterial efficacy of the final combination material, ePTFE-20, was assessed with a 4 h adhesion study against gram-positive *Staphylococccus* aureus (*S. aureus*) and gram-negative *Escherichia coli* (*E. coli*). It is expected that ePTFE-20 will prevent infection and adhesion of fouling agents and remain cytocompatible throughout the aforementioned studies.
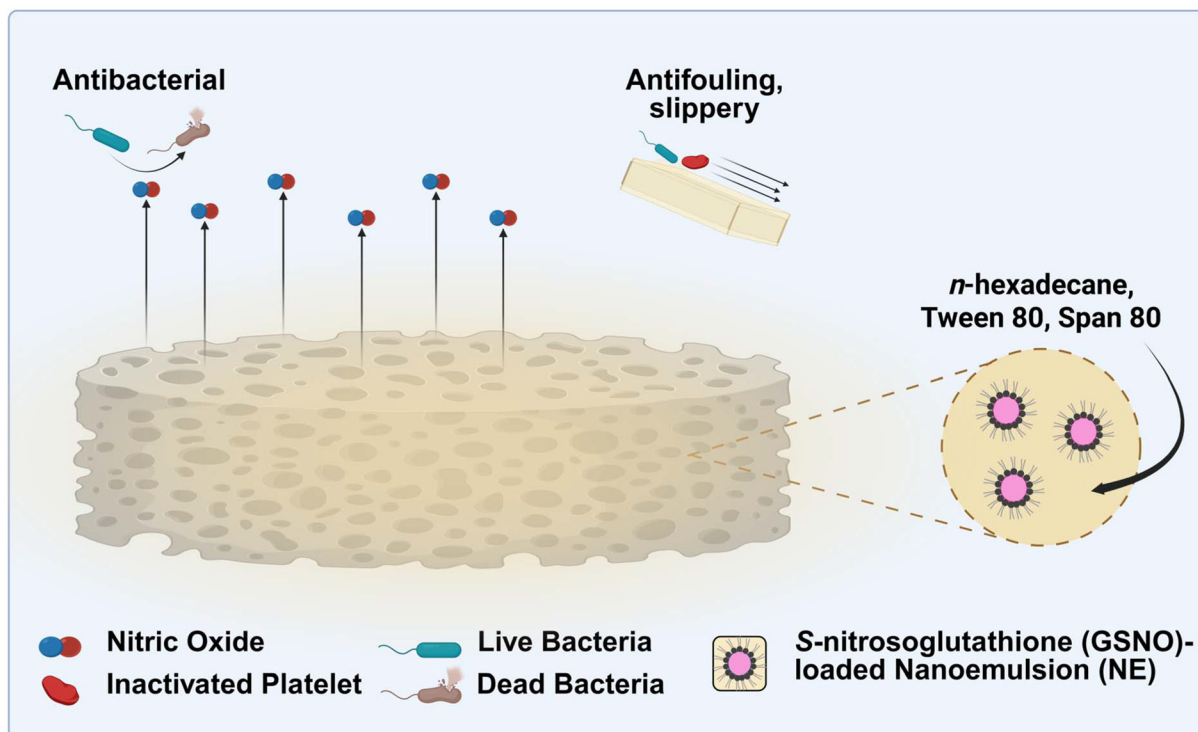
2. Materials & methods

2.1. Materials

Sodium nitrite (≥97%), hydrochloric acid (37%), acetone (≥99.9%), polyoxyethylene (20) sorbitan monooleate (Tween 80), sorbitan monooleate (Span 80), *n*-hexadecane (99%), thiazolyl blue tetrazolium bromide 98%, (4-(2-hydroxyethyl)-1-piperazineethanesulfonic acid) (HEPES buffer), and Luria Bertani (LB) broth media and agar were purchased from Sigma Aldrich (St. Louis, MO). Reduced L-glutathione was purchased from Gold Bio (St. Louis, MO). All aqueous solutions were prepared using deionized water. Phosphate buffer saline (PBS) 10 mM with 100 μM EDTA was used for all material characterization and NO analyzer studies. Calcium and magnesium-free PBS (CMF-PBS, 1x) was purchased from Corning Incorporated (Manassas, VA). Dulbecco's Modified Eagle Medium (DMEM), fetal bovine serum (FBS), and penicillin–streptomycin (P/S) were purchased from VWR (Radnor, PA). The lactic dehydrogenase (LDH) kit was purchased from Roche Life Sciences (Indianapolis, IN). Drabkin's reagent was acquired from Ricca Chemical Company (Arlington, TX). Bacterial strains *Escherichia coli* (*E. coli*, ATCC 25922), *Staphylococcus aureus* (*S. aureus*, ATCC 6538), and 3T3 mouse fibroblast cells (ATCC 1658) for cell compatibility were obtained from American Type Culture Collection (ATCC, Manassas, VA). Primary human umbilical vein endothelial cells (HUVEC) were obtained from Gibco under Thermo Fisher Scientific (Waltham, MA). EGM-2 Endothelial Cell Growth Medium-2 BulletKit was purchased from Lonza (Walkersville, MD). Fresh porcine whole blood was acquired from the University of Georgia Swine Unit (Athens, GA).

2.2. *S*-Nitrosoglutathione (GSNO) synthesis

S-Nitrosoglutathione was synthesized according to an established protocol.[46] Briefly, reduced L-glutathione (900 mg) was dissolved in 2 M HCl (1.25 mL) and DI water (4 mL) and

Fig. 1 Material design of the GSNO-loaded nanoemulsion infused into expanded polytetrafluoroethylene. The NO release and slippery capability of the GSNO-NE–infused substrate will repel biofouling agents as well as prevent bacterial infection from propagating.

stirred for 10 min over an ice bath. To nitrosate the solution, sodium nitrite (215 mg) was added and protected from light. The solution was allowed to stir and chill in an ice bath for 40 min. Then, chilled acetone (5 mL) was added to the solution and allowed to stir for another 10 min. The solution was filtered *via* vacuum filtration, and the precipitate was washed with chilled DI water and acetone to remove any unreacted sodium nitrite. The resultant GSNO was dried for 12 h *via* vacuum desiccation, ground down with a mortar and pestle, and stored at −20 °C protected from light.

2.3. Nanoemulsion (NE) – infused expanded polytetrafluoroethylene (ePTFE) sample preparation

2.3.1. GSNO-NE fabrication. The nanoemulsion (NE) was synthesized by modifying a protocol from Agarwal *et al.*[43] First, polyoxyethylene (20) sorbitan monooleate (Tween 80, 7.5 parts by weight) and sorbitan monooleate (Span 80, 22.5 parts by weight) were dissolved in *n*-hexadecane (70 parts by weight) and vortexed for 1 min to mix thoroughly. The oil-surfactant solution was vacuum filtered through a 0.1 μm PTFE filter and stored at room temperature.

Two formulations of the GSNO-NE were prepared: NE-20, a NE loaded with a 20 mg mL^{-1} GSNO solution in the aqueous phase, and NE-25, a NE loaded with a 25 mg mL^{-1} GSNO solution in the aqueous phase. Both GSNO solutions were prepared by dissolving GSNO in 10 mM PBS with 100 μM EDTA. The GSNO solution was added to a glass vial (5% v/v), and the oil-surfactant solution was slowly pipetted into the glass vial at a

rate of 200 μL per 20 s with magnetic stirring at 700 rpm. Once the oil-surfactant solution was roughly incorporated, NE-20 and NE-25 were sonicated *via* an ultrasonic probe (Split Type Ultrasonic Processor, Vevor, Shanghai, China, 50%, 19.5 kHz) for 2.5 min on an ice bath. Finally, the GSNO-NEs were allowed to stir at 700 rpm for 1 h protected from light to stabilize the solution.

2.3.2. Dynamic light scattering (DLS). To confirm the fabrication of a nanoemulsion, the hydrodynamic diameter of the GSNO-NE droplets was measured using Dynamic Light Scattering (DLS). The GSNO-NEs were diluted with *n*-hexadecane in a 1 : 200 ratio; the diluted GSNO-NEs were processed with the Zetasizer Nano ZS (Malvern Panalytical, Malvern, Worcestershire, United Kingdom) over 3 measurements to confirm the formation of a nanoemulsion (with hydrodynamic diameters <200 nm).

2.3.3. Polymer-nanoemulsion infusion. To determine an adequate infusion duration for the GSNO-NEs to swell into the expanded polytetrafluoroethylene (ePTFE), the swelling ratio and rate were calculated. The initial mass of the unswelled ePTFE ($n = 6$) was measured and recorded. Next, the ePTFE samples were immersed in a NE with GSNO loaded for set periods. At each time point, the ePTFE was removed from the NE, weighed, and immersed in the NE again for a total of 4 h. Then, the swelling ratio and rate were calculated according to eqn (1) and (2), respectively, where m_x is the weight of the sample at a certain time point, $m_{initial}$ is the initial weight of the sample prior to immersion in the NE, ΔSR is the change in

Biomaterials Science

swelling ratio, and Δtime is the change in time. The swelling ratio and rate stabilized after 30 min; therefore, all following sample preparation swells the ePTFE in NE (*i.e.* ePTFE-NE, ePTFE-20, ePTFE-25) for 30 min for future studies.

$$\text{Swelling ratio (SR)} = \frac{m_x}{m_{\text{initial}}} \tag{1}$$

$$\text{Swelling rate} = \frac{\Delta \text{SR}}{\Delta \text{time}} \tag{2}$$

2.4. Scanning electron microscopy (SEM) and energy-dispersive X-ray spectroscopy (EDS)

The surface and the cross-section of various ePTFE samples were observed under the Hitachi SU3900 Scanning electron microscope (SEM). For bacterial imaging, the samples were first coated with a 10 nm gold-palladium coating using a Leica EM ACE200 sputter coater (Buffalo Grove, IL). The samples were scanned under variable pressure with an accelerating voltage of 10–20 kV. Whenever applicable, the elements present on the surface of the sample were determined using energy-dispersive X-ray spectroscopy (EDS, Oxford Instruments).

2.5. Bacteria sample preparation for SEM

The surface of the bacteria-exposed ePTFE samples were observed under SEM after extensive preparation. In short, bacteria-exposed samples were rinsed in PBS and incubated in a 2% glutaraldehyde solution overnight to fix the bacteria on the surface of the samples. Next, the samples were incubated in 0.1 M HEPES buffer for 15 min. Then, the samples were dehydrated by soaking them in different concentrations of an ethanol solution (50, 70, 95, 100%) sequentially for 20 minutes each. Finally, the samples were dehydrated further by soaking them in an ethanolic mixture of hexamethyldisilazane (HMDS) for 15 minutes, after which the samples were allowed to dry overnight before imaging.

2.5.1. Pore size distribution analysis. The SEM images were analyzed using the digital image analyzing software ImageJ for the pore size distribution of the ePTFE, ePTFE-NE, ePTFE-20, and ePTFE-25. The pores on the surface of each sample were isolated, and the area of each pore was calculated and averaged. The percent porosity was then determined based on the size of the image.

2.6. GSNO loading

As the aqueous phase of the nanoemulsions were determined on a v/v basis, determining the GSNO loaded into the NE is beneficial. To do so, unswelled ePTFE was weighed, and NE-20 and NE-25 were swelled into the ePTFE samples. After 30 min, the ePTFE-20 and ePTFE-25 ($n = 4$) samples were weighed again; the weight change was equated to the weight of the GSNO-NE swelled into the polymer matrix. The NE-20 and NE-25 swelled into the ePTFE were then diluted in 100% ethanol (1 mL), as *n*-hexadecane is soluble in ethanol, and incubated at room temperature for 1 h. The molar absorptivity

(ε) of GSNO in 100% ethanol was determined to be 1360.4 M^{-1} cm^{-1} at a wavelength of 340 nm. The absorbance of the dilutions was then measured using an Agilent Cary 60 UV-vis spectrometer (Agilent Technologies, Santa Clara, CA) at 340 nm. The absorbance was equated to a concentration of GSNO *via* Beer-Lambert's Law, and the amount of GSNO swelled into the ePTFE was calculated.

2.7. GSNO leaching

As GSNO is a molecule that is sometimes prone to diffusing from its bulk material reservoir, a leaching study was conducted. Briefly, ePTFE-20 and ePTFE-25 ($n = 4$) were prepared according to Section 2.3.3; the samples were then immersed in 10 mM PBS with 100 μM EDTA (2 mL), herein referred to as leachates, for set time points. The molar absorptivity (ε) of GSNO in the PBS with EDTA was determined to be 403.9 M^{-1} cm^{-1} at a wavelength of 340 nm. At each time point, the absorbance of the leachates was also measured using an Agilent Cary 60 UV-vis spectrometer (Agilent Technologies, Santa Clara, CA) at 340 nm, and the cumulative GSNO leached over 24 h was calculated. The samples were measured at various time points for up to 24 h.

2.8. Water contact angle

The static water contact angle (WCA) of a material's surface gives insight into the wettability of the substrate. The WCA of ePTFE, NE-swelled, and GSNO-NE-swelled samples were measured with a Contact Angle Goniometer (Ossila Ltd, Sheffield, England). Briefly, all control and test groups ($n = 3$) were measured by placing the samples on the leveled goniometer stage. A 5 μL water droplet was placed on the sample, allowed to stabilize, and the WCA was measured in the Ossila Contact Angle software and recorded. This was repeated 2 more times per technical replicate.

2.9. Initial sliding angle

The sliding angle of a surface gives insight into the surface's slippery behavior. Therefore, the sliding angle on ePTFE, ePTFE-NE, ePTFE-20, and ePTFE-25 ($n = 4$) were all measured. The samples were placed on a digital protractor. A droplet of dyed water was placed on the surface, and the sample was tilted until the droplet began to move. The angle that the tilting stage made with the horizontal was recorded as the sliding angle.

2.10. NE coating stability

While the initial sliding angle exhibits a surface's initial slippery abilities, the sliding angle over time is more indicative of the surface's ability to retain its slippery behavior. The stability of the NE coating of ePTFE-20 and ePTFE-25 ($n \geq 4$) was assessed by measuring the sliding angle of the surface after incubation in physiological conditions (10 mM PBS with 100 μM EDTA, 37 °C) for set time points up to 30 d. Similarly to section 2.9, the samples were placed on a digital protractor with a droplet of dyed water on the surface, and the sliding

angle was measured and recorded. After each time point, the samples were placed in PBS at 37 °C.

2.11.   Nitric oxide (NO) release profile

2.11.1.   24 h NO release. The nitric oxide (NO) release from the ePTFE-20 and ePTFE-25 samples were evaluated using the gold standard Zysense Nitric Oxide Analyzer (NOA) 280i (Frederick, CO) *via* chemiluminescence detection method. The NO-releasing samples were first submerged in 10 mM PBS with 100 µM EDTA at 37 °C. A nitrogen bubbler and sweep gas were placed in the solution at a flow rate of 200 mL min^{-1} to release any NO trapped in the liquid phase and sweep the gas into the NOA. The samples' NO release was measured until the release stabilized. The samples were then incubated in 10 mM PBS with 100 µM EDTA at 37 °C protected from light between time points. The NO-releasing samples were measured at 4 h and 24 h after GSNO-NE infusion.

2.11.2.   NO release after 30 min UV sterilization. The NO release of ePTFE-20 and ePTFE-25 were measured after 30 min of UV sterilization, a sterilization technique used in the following biological experiments. The prepared samples were UV sterilized for 30 min, 15 min on each side. Following sterilization, the same protocol was followed as in section 2.11.1. The NO-releasing samples were measured until the release reached a steady state.

2.12.   Cytocompatibility evaluation

Cell cytocompatibility was assessed for the ePTFE-20 samples using NIH 3T3 mouse fibroblast cells and human umbilical vein endothelial cells (HUVEC) per the ISO 10993-5 standard.[47] Briefly, the 3T3 cells were revived and cultured in DMEM supplemented with 10% fetal bovine serum and 1% penicillin streptomycin (complete DMEM) while the HUVECs were cultured in EBM-2 with supplements (complete EBM-2). The cells were seeded on a 96 well plate at a cell seeding density of 1×10^4 cells per well (3T3) or 5×10^3 cells per well (HUVEC) and incubated at 37 °C, 5% CO_2 for 24 h.

The ePTFE, ePTFE-NE, and ePTFE-20 samples ($n = 4$) were sterilized with 70% ethanol and UV sterilized for 30 min (15 min on each side). The samples were then incubated in complete DMEM (1 mL) for 3T3 cells or complete EBM-2 (1 mL) for HUVECs as the extraction medium for 24 h at 37 °C, 5% CO_2. The cells seeded on the 96 well plate were then exposed to the leachates for 24 h at 37 °C, 5% CO_2.

The MTT colorimetric assay was used to determine the metabolic activity of the cells after exposure to sample leachates. The leachates were removed from the wells and replaced with the working MTT solution (0.5 mg mL^{-1}, 100 µL) and incubated at 37 °C, 5% CO_2 for 2.5 h (3T3) or 4 h (HUVEC). Then, the MTT working solution was replaced with DMSO (100 µL) to redissolve the formazan crystals formed and agitated on an orbital shaker for 10 min to ensure thorough dissolution of the crystals. The absorbance of the plates were read on a BioTek Cytation 5 Imaging Reader (Winooski, VT) at 570 nm and 690 nm reference wavelength. The relative cell viability was calculated according to eqn (3), where ABS$_{sample}$ is

the absorbance of the cells exposed to test sample leachates (*i.e.*, ePTFE, ePTFE-NE, and ePTFE-20), ABS$_{untreated}$ is the absorbance of the untreated cells, and ABS$_{blank}$ is the absorbance of the 96-well plate with DMSO.

$$\text{Relative cell viability} (\%) = \frac{\text{ABS}_{sample} - \text{ABS}_{blank}}{\text{ABS}_{untreated} - \text{ABS}_{blank}} \times 100 \quad (3)$$

2.13.   Hemocompatibility assessment

The hemolytic effects of the GSNO-NE-infused ePTFE samples were assessed against its control using a direct contact approach according to the ISO 10993-4 standards.[48] Briefly, porcine whole blood was diluted with calcium- and magnesium-free PBS (CMF-PBS) to a working hemoglobin concentration of 10 mg mL^{-1}, referred to as dilute whole blood (DWB). The samples ($n = 6$) and high-density polyethylene (HDPE, $n = 3$) were incubated in DWB in an extraction ratio of 3 cm^2 mL^{-1} per the ISO standard for 3 h at 37 °C with manual inversion every 30 min. Simultaneously, DWB (1 mL) was incubated in deionized water (7 mL) as the positive control and CMF-PBS (7 mL) as the blank. After the 3 h incubation, the samples were removed, and the DWB was centrifuged to obtain a supernatant and blood cell pellet. The supernatant was reacted with Drabkin's reagent in a 1:1 ratio for 15 min at room temperature, and the absorbance was read at 540 nm on a BioTek Cytation 5 Imaging Reader (Winooski, VT).

A standard curve of porcine hemoglobin was also reacted with Drabkin's reagent in a 1:1 ratio, and the absorbance was read at 540 nm on the plate reader. Final results were calculated using eqn (4) and (5), where [Hgb]$_{sample}$ is the concentration of hemoglobin in the supernatant of DWB incubated with samples, [Hgb]$_{blank}$ is the concentration of hemoglobin in the DWB, and [Hgb]$_{total}$ is the concentration of hemoglobin in the positive control.

$$\%\text{Hemolysis} = \frac{[\text{Hgb}]_{sample} - [\text{Hgb}]_{blank}}{[\text{Hgb}]_{total}} \times 100 \quad (4)$$

$$\text{Hemolytic index} = \%\text{hemolysis}_{sample} - \%\text{hemolysis}_{HDPE} \quad (5)$$

2.14.   Fibrinogen adsorption evaluation

As a prevalent blood protein in the clotting cascade, fibrinogen (Fg) adsorption was assessed on the samples through the incubation of FITC-labeled Fg (FITC-Fg). Briefly, the ePTFE, ePTFE-NE, and ePTFE-20 samples were prepared according to section 2.3.3. Once swelled with the respective NEs, the samples were incubated with CMF-PBS at 37 °C for 1 h to reach surface saturation. After 1 h, a background scan was measured on a Biotek Cytation 5 Imaging Reader (Winooski, VT) with excitation at 490/20 and emission at 525/20. While the background scan was collected, a working solution of Fg (4 mg mL^{-1}) was prepared, consisting of 1:10 FITC-Fg to unlabeled Fg.

Without removing the initial CMF-PBS, the samples were then incubated in the diluted Fg solution (100 µL) at 37 °C for 90 min. Simultaneously, a standard curve was prepared with

the diluted Fg in a 1 : 1 serial dilution and incubated in the same conditions. After the incubation, each sample well was washed with fresh CMF-PBS several times (8–25 times) to ensure non-adsorbed Fg was removed from the sample. Finally, the fluorescence intensity was read on the Biotek Cytation 5 Imaging Reader (Ex: 490/20, E*m*: 525/20), and the Fg adsorbed was calculated and normalized to the sample surface area. Fluorescent images of the Fg were taken using an Advanced Microscopy Group's EVOS FL Fluorescence Imaging Microscope (AMG, Mill Creek, WA). The final results are reported as a mean ± standard deviation ($n = 8$, $p < 0.05$).

2.15. Antibacterial efficacy assessment

The antibacterial efficacy of the fabricated samples was tested through a 4 h adhesion assay against *S. aureus* and *E. coli*. For the bacterial assay, a single colony of either *S. aureus* or *E. coli* was isolated and grown in LB media at 37 °C for 8 h. After the bacteria was at the log phase of growth, the bacterial solution was centrifuged to obtain a bacterial pellet. Then, the pellet was washed with PBS and diluted to obtain a concentration of 10^8 CFU mL^{-1}.

All three sample types were sterilized under UV light for 30 min. Then, the samples were incubated in the diluted bacteria solution in a 24-well plate, The well plate was then protected from light and incubated at 37 °C for 24 h while shaking at 150 rpm. After 24 h, the samples were removed from the suspension and rinsed with PBS. Then the samples were homogenized for 1 min using an Omni-TH homogenizer (Omni, Kennesaw, GA) followed by vortexing for 1 min. The solution was then diluted and plated on a LB agar Petri dish using an Eddy Jet 2 W bacteria spiral plater (IUL instruments, Barcelona, Spain). The plates were incubated at 37 °C for 24 h, and the individual colonies were counted using a SphereFlash Automatic Colony Counter (IUL Instruments, Barcelona, Spain). The reduction in the viability of adhered bacteria was calculated using eqn (6) where $C_{control}$ represents the colonies of bacteria in CFU cm^{-2} on the control ePTFE and C_{sample} represents the colonies of bacteria in CFU cm^{-2} on the test samples (*i.e.*, ePTFE-NE and ePTFE-20):

$$\%\text{Viable bacterial reduction} = \frac{C_{control} - C_{sample}}{C_{control}} \times 100 \quad (6)$$

2.16. Statistical analysis

All experiments were performed with $n \geq 3$ samples, and One-Way ANOVA was used to determine statistical significance in GraphPad Prism. Final results are all reported as mean ± standard deviation.

3. Results & discussion

3.1. Fabrication of GSNO-NE swelled ePTFE

To incorporate the GSNO directly into the NE, rendering the NE as NO-releasing, 20 mg mL^{-1} and 25 mg mL^{-1} solutions of GSNO, with a purity of 96.51% (Fig. S1), were prepared in PBS

with EDTA and used as the aqueous phase of the NE. These concentrations of GSNO were chosen due to the solubility limit of the molecule in aqueous media being around 20 mg mL^{-1}; GSNO can easily be solubilized at a concentration of 20 mg mL^{-1} while taking more agitation and time to dissolve at 25 mg mL^{-1}.[49] This additional agitation could cause premature molecule degradation and lead to loss of NO.
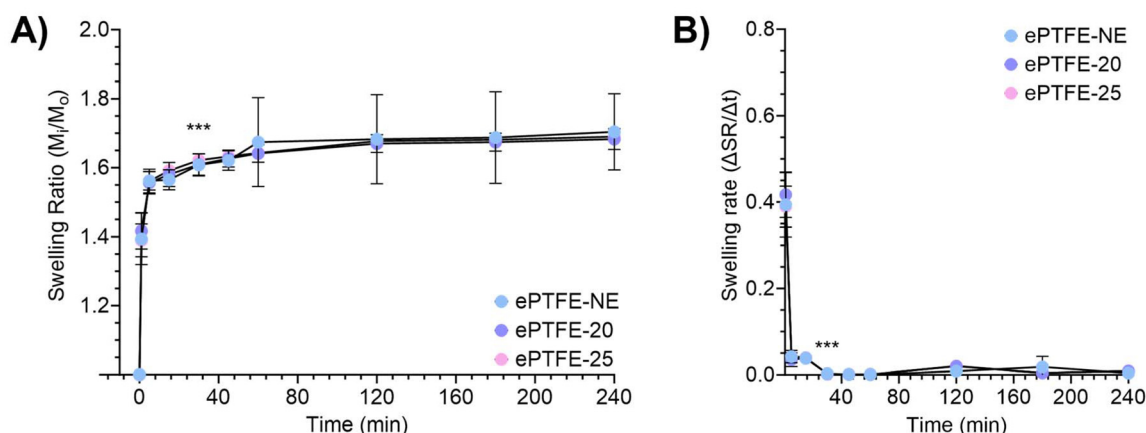
In addition to the limitation of the solubility of GSNO, the NE system itself had a physical limitation. Only 5% (v/v) of the total NE was composed of the NO donor solution, limiting the finite supply of the NO donor GSNO. While increasing the volume percentage of the aqueous phase (*e.g.* 10% v/v) would increase the total amount of GSNO loaded into the NE and thereby prolong NO release, the dispersed surfactant-protected micelles become unstable, begin to flocculate and coalesce, and cause phase separation. Therefore, all experiments proceeded with the lower volume percentage. The resulting NEs with 20 mg mL^{-1} and 25 mg mL^{-1} GSNO solutions dispersed in them, herein referred to as NE-20 and NE-25, respectively, retained a translucent yellow appearance with a slight pink tinge due to the pink GSNO (Fig. S2).

Although the solutions did not exhibit any visible aggregates, the formation of a NE was verified by dynamic light scattering (DLS), which is based on the principle of Brownian motion. Brownian motion refers to the random movement of particles, especially particles suspended in a fluid, when the particles collide with one another.[50,51] Dynamic light scattering serves to track the light scattered due to the Brownian motion of the nano-droplets within the NEs and measure the hydrodynamic diameter of those nano-droplets. Dynamic light scattering indicated that NE-20 and NE-25 had hydrodynamic diameters of 70.60 ± 2.14 nm and 85.52 ± 0.48 nm, respectively, confirming that nanoemulsions had been formed (Fig. S3).

Once the formation of NEs were confirmed, the NE-20 and NE-25 were swelled into ePTFE, herein referred to as ePTFE-20 and ePTFE-25, respectively. It was determined through the swelling ratio and rate of ePTFE (Fig. 2A and B) that 30 min would sufficiently and fully swell the ePTFE; the mass of the ePTFE did not significantly increase after that time point. As an expanded version of typical PTFE, ePTFE is much more porous, lending to the overall ability of the material to readily swell hydrophobic solutions at a relatively fast rate. Although more porous, the inherent properties of PTFE are retained within ePTFE, such as the hydrophobicity and inability to swell aqueous media.

Due to the hydrophobic and chemically inert nature of fluorinated polymers like PTFE and ePTFE, it has been historically challenging to incorporate a bioactive molecule into the matrix. Specifically, RSNOs like GSNO or SNAP tend to be difficult to blend or impregnate directly into fluoropolymers due to their hydrocarbon base's high polarity interfering with the fluorocarbon base.[52] Recent reports demonstrate the modification of RSNOs with complex fluoro-chemistry to fluorinate the molecules for incorporation into fluorinated polymers.[53] One such molecule in particular, fluorinated SNAP, was modi-

Fig. 2 Swelling (A) ratio and (B) rate of ePTFE samples. Since the ePTFE, which is inherently hydrophobic, was especially porous, it was able to swell the hydrophobic NE within 30 min with no significant change in weight after that time ($n = 6$, ***$p < 0.001$).

fied to allow solvent impregnation into polyvinylidene fluoride (PVDF).[52,54] Essentially, the group fluorinated the SNAP precursor D-penicillamine and nitrosated the molecule in a multistep process over several days, adding to the complexity of the fabrication of the overall material.

The present method for the incorporation of GSNO, a similar RSNO to SNAP, into the fluorinated polymer ePTFE reduces the complexity of the fabrication and eliminates the need for complex fluoro-chemistry. Rather than taking several days to synthesize a modified product, the fabrication of the GSNO-NE and subsequent swelling into the ePTFE can be completed within 24 h. This fabrication scheme takes an unmodified, well-studied NO donor and disperses it within a nanoemulsion. Here, GSNO is present only in small volumes in the form of nano-droplets that are scattered throughout a hydrophobic oil, n-hexadecane; therefore, its hydrocarbons and aqueous phase do not interfere with the fluorocarbons of ePTFE and are integrated into the polymer matrix easily. As similar characteristics tend to gravitate toward each other, the GSNO-loaded hydrophobic n-hexadecane-based nanoemulsion was readily swelled into the equally hydrophobic ePTFE through capillary action, thus resulting in a much easier scheme to incorporate a RSNO in a fluoropolymer.

3.2. Surface characterization

Energy Dispersive X-ray spectroscopy (EDS) was conducted on ePTFE, ePTFE-NE, ePTFE-20, and ePTFE-25. Unsurprisingly, fluorine was the most detected element across all sample types as the base ePTFE is composed of only fluorine and carbon (Fig. S4). With the introduction of the NE and GSNO-NE, there is an increase in the presence of carbon and an emergence of the presence of oxygen. This is due to the NE itself, which is composed of carbon-rich n-hexadecane, Tween 80, and Span 80 which both have oxygen present.

The surface morphology of the ePTFE, ePTFE-NE, ePTFE-20, and ePTFE-25 were imaged using scanning electron microscopy (SEM) and exhibited some fibrous structures with

porosity (Fig. S5). From these images, the porosity of the samples was analyzed using the digital image analyzing software ImageJ. The percent porosity of the control ePTFE was $0.09 \pm 0.22\%$ while the NE-swelled samples exhibited a reduction in porosity by about 22.22% (Table S1). Although there was a decrease in the porosity between control ePTFE and swelled ePTFE, that loss likely indicates and confirms the swelling and presence of the NE within the ePTFE matrix. The loss of porosity does not affect the overall slippery behavior or NO release profile as seen with the experiments following the swelling.

3.3. NE coating characterizations

3.3.1. Water contact angle. The water contact angle of the ePTFE, NE-swelled, and GSNO-NE-swelled samples were measured and compared to non-expanded PTFE. The PTFE, ePTFE, and ePTFE swelled with n-hexadecane all exhibited water contact angles greater than 100° (Fig. S6), indicating the retention of hydrophobicity. However, with the inclusion of the NE or GSNO-NE into ePTFE, the water contact angle of ePTFE-NE, ePTFE-20, and ePTFE-25 decreased to ~50°, similar to previous literature.[55] This is most likely due to the presence of hydroxyl groups in the surfactants Tween 80 and Span 80 that make up the NE micelles. The hydroxyl groups tend to impart hydrophilicity on surfaces which would reduce the water contact angle.[56] In terms of surface biofouling, the NE-swelled samples are still expected to prevent foulants from adhering to the sample surface regardless of the reduced water contact due to the low surface tension of the bulk n-hexadecane.[55,57] Low interactions between the lubricant and fouling agents would promote the anti-fouling behavior. Despite the decrease in water contact angle, the oil itself maintains slippery behavior as seen in further experiments.

3.3.2. Slippery behavior assessment. The slippery behavior of the GSNO-NE infused ePTFE samples was characterized by measuring the sliding angle of the samples. Sliding angle is the measure of the angle at which a liquid droplet begins to

slide from a surface; typically, the sliding angle of a surface must be less than 20° in order to be considered a slippery surface. Therefore, the initial sliding angle was measured *via* a digital protractor. As ePTFE itself is somewhat of a hydrophobic surface, it inherently has some anti-fouling characteristics, such as a lower sliding angle (Fig. 3A). However, with the introduction of a NE swelled into the polymer matrix, the sliding angle decreased even further due to the lubricant layer on the surface (Fig. 3A). The difference in surface tensions between the NE base *n*-hexadecane (27.47 mN m^{-1}) and water (72.80 mN m^{-1})[57,58] attributed to the ease at which the water slides off of the lubricant surface. Since the NE has a lower surface tension, it is more prone to spreading and allowing for the water droplet that is more prone to beading up to slide off of the surface.

The anti-fouling effect from the NE-swelled surfaces was not concentration-dependent with respect to the GSNO concentration. These higher concentrations of GSNO were chosen for observation because the GSNO solution that was incorporated into the NE is a very small amount (5% v/v) and would have a shorter NO release profile. Therefore, the NO released was maximized by maximizing the GSNO concentration. Incorporating lower concentrations of the GSNO solution into the NE would not affect the slippery behavior as it is present in a very low amount within the NE, and the anti-fouling behavior mainly comes from the low surface tension of the *n*-hexadecane-based NE itself.[57,58] As a proof-of-concept, the ePTFE-NE has no GSNO loaded into the NE and still exhibited slippery behavior for the duration of the study.
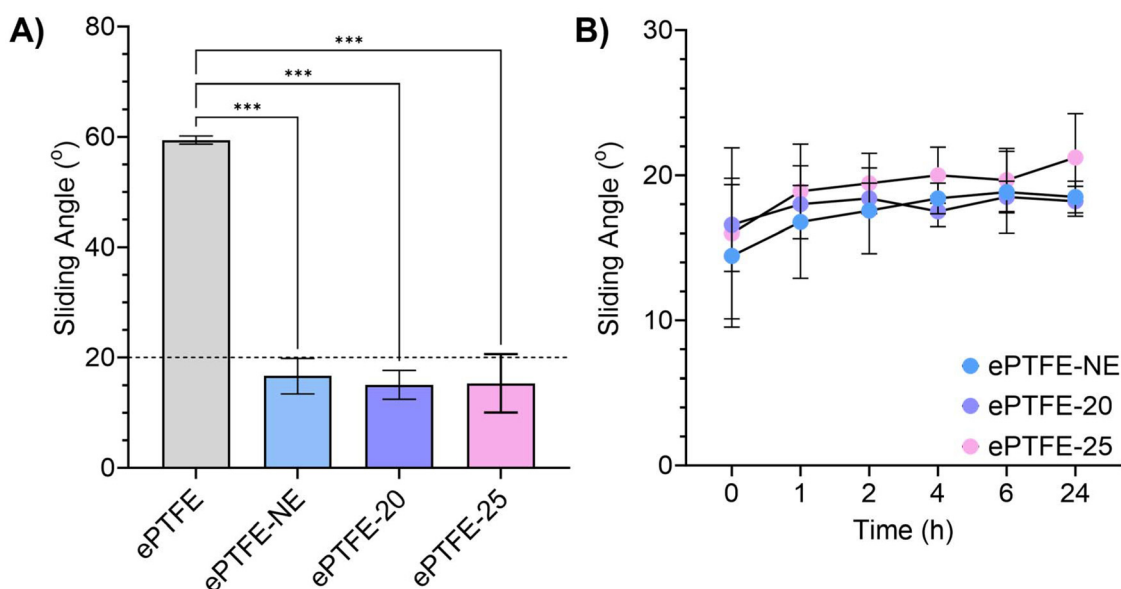
While the initial sliding angle measurements are beneficial to understanding the surface characteristics upon fabrication, the NE coating stability gives an insight into the durability of the material. As the onset of infection and device failure due to bacterial attachment and the foreign body response (FBR) in the first 24 h after a surgical procedure is the most critical,[59,60] the slippery behavior was focused on that time duration. The NE coating stability was characterized by sliding angle measurements after sample incubation in 10 mM PBS with 100 μM EDTA at 37 °C. At each time point, the sliding angle remained below 20°, indicating the proclivity towards anti-fouling behavior (Fig. 3B). The sliding angle at longer time points also suggest prolonged anti-fouling behavior with sliding angles near 20° for 30 d (Fig. S7).

3.4. NO loading and release

3.4.1. GSNO loading and leaching. Primary and tertiary RSNOs have been previously incorporated into various medically relevant biomaterials,[16–21,61] but none of the reported methods incorporated the RSNOs in low amounts that were still effective against bacterial activity. Typically, a high concentration of NO due to a substantial amount of NO donor must be present to contribute a bactericidal effect.[62–64] The RSNOs reported previously also have varying levels of stability in physiological conditions due to the nature of their structure and state within a polymer matrix. Tertiary donors are present in both an amorphous and a crystalline state, allowing for a stable and controlled release of NO, while primary donors do not necessarily have a crystalline form for additional stability. Although primary RSNOs are typically less stable than tertiary donors, the endogenous GSNO is among the more stable primary donors, leading to greater biocompatibility.[28–30]

In the present work, the primary NO donor GSNO was incorporated into the NE as an aqueous solution (20 mg mL^{-1} and 25 mg mL^{-1}) that made up 5% v/v of the total NE volume.

Fig. 3 (A) Initial sliding angle of the GSNO-NE-infused ePTFE samples and their controls. As observed, ePTFE alone has some level of slip; however, in introduction of the NE into the polymer matrix further decreased the sliding angle below 20 (n = 4, ***p < 0.001). (B) NE coating stability over 24 h. The slippery behavior of the NE-infused samples was maintained even after incubation at physiological conditions ($n \geq 6$, p > 0.05).
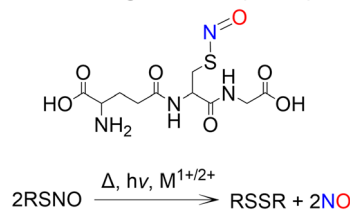
The NE-20 and NE-25 swelled into ePTFE was diluted with 100% ethanol to solubilize the *n*-hexadecane and GSNO to prevent a colloidal suspension from interfering with absorbance measurements. Unsurprisingly, the GSNO loaded into ePTFE-25 (65.03 ± 1.69 μg cm^{-1}) was significantly higher than that of ePTFE-20 (43.43 ± 2.88 μg cm^{-1}) by about 49.74% (Fig. 4A) due to the higher concentration of GSNO that was incorporated into NE-25. Interestingly, however, the samples exhibited a similar GSNO diffusion profile (Fig. 4B), indicating that the higher concentration of GSNO incorporated into NE-25 and ePTFE-25 does not necessarily equate to higher rates of molecule diffusion. This may be attributed to the material environment that the GSNO is encapsulated in. To load the GSNO into the NE and subsequently swell it into ePTFE, it is dissolved in an aqueous media and thoroughly dispersed throughout hydrophobic *n*-hexadecane. Once encapsulated in the oil and protected by surfactant micelles, the GSNO-NE can be easily swelled into hydrophobic ePTFE. However, for the whole GSNO molecule, which is relatively hydrophilic comparatively, to diffuse out from the aqueous droplets, it must attempt to diffuse through both the hydrophobic oil and the hydrophobic polymer matrix. Both materials would essentially block the molecule since they do not have an affinity for each other. Therefore, it is hypothesized that the diffusion of GSNO from the polymer matrix is mainly governed by the material environment rather than the amount loaded. Both ePTFE-20 and ePTFE-25 were nearly depleted of GSNO by the end of 24 h, pointing towards the insignificance of using the higher concentration ePTFE-25 altogether. Since the rates for ePTFE-20 and ePTFE-25 were similar, it can be expected that the NO release profile may be similar as well.

3.4.2. NO release. The structure of NO donors lends itself to the rate and stability at which NO is released. As a primary RSNO, GSNO readily severs its S–NO bond to release NO through hydrolysis, heat, meta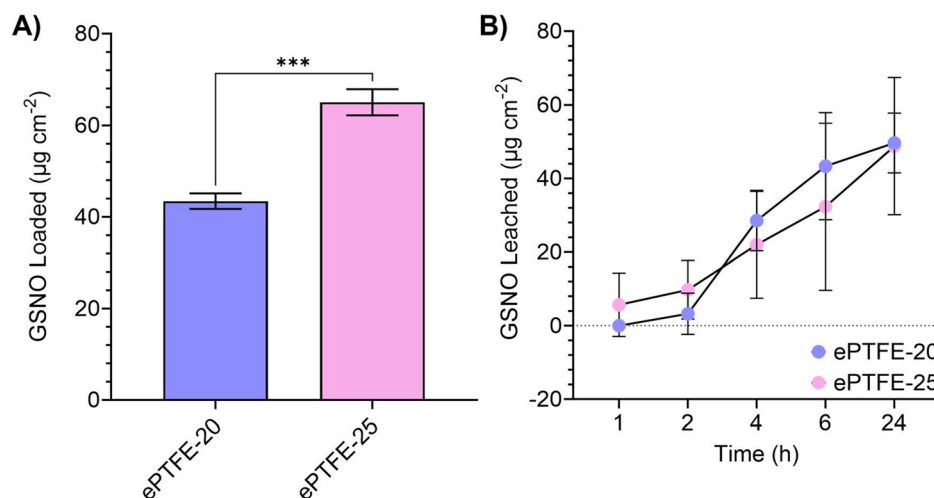l ion interaction, or light cataly-sis (Scheme 1). However, when protected by a hydrophobic oil and surfactant micelle in the NE, external hydrolysis is prevented, and the release of NO from GSNO is steadier. The rate at which the NO released from the GSNO-NE-infused ePTFE samples was evaluated using the gold standard chemiluminescence detection of a Nitric Oxide Analyzer (NOA) over the course of 24 h.

The ePTFE-20 and ePTFE-25 samples were freshly prepared prior to the initial NO release measurement in the NOA. For the duration of the experiment, the samples were incubated in 10 mM PBS w/100 μM EDTA at 37 °C and protected from light. As an aqueous solution, the GSNO immediately released NO while incorporated into the NE. Therefore, the NO measured at hour 0 is an average of the NO released from fabrication to measurement. Once exposed to physiological conditions at hour 0, the NO release from both sample types was found to be around 0.4×10^{-10} mol min^{-1} cm^{-2}. While this is on the lower end of physiological concentrations of NO ($0.5–4 \times 10^{-10}$ mol min^{-1} cm^{-2}),[65] the ePTFE-20 and ePTFE-25 samples continued to release at sub-physiological levels for 24 h, between 0.08 and 0.1×10^{-10} mol min^{-1} cm^{-2} (Fig. 5A). These lower levels of NO release (ranging from picomolar levels[32] to 500

Scheme 1 The molecular structure of GSNO and its NO release mechanisms through thermal, photo-, and metal ionic catalysis.

Fig. 4 (A) GSNO loading ($n = 3$, ***$p < 0.001$). (B) GSNO leaching ($n = 3$, $p > 0.05$). While the GSNO loaded into the ePTFE-25 sample was significantly higher than that of ePTFE-20, the leaching profiles are similar. Nearly all of the GSNO loaded into the NE and infused into the ePTFE was depleted after 24 h.
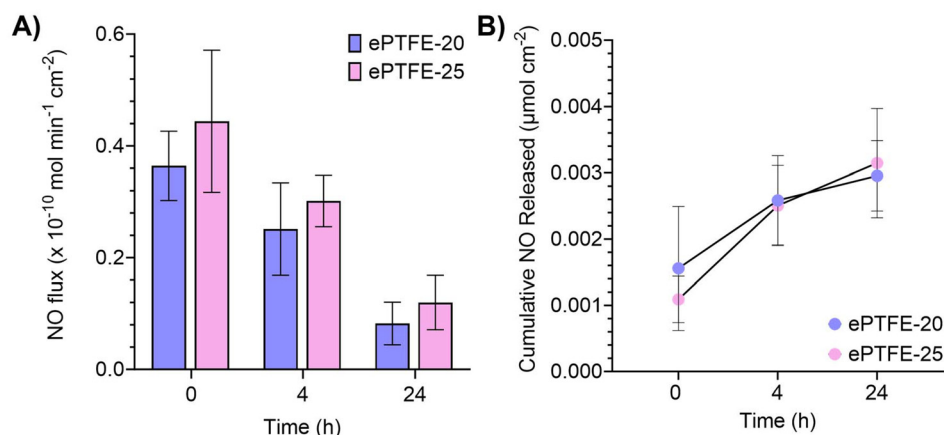
Fig. 5 (A) NO release over 24 h. (B) Cumulative NO released. Between both concentrations of GSNO loaded into the NE and infused into the ePTFE, there was no significant difference seen in the level of NO release. This is corroborated by the amount of GSNO diffused over 24 h ($n \geq 5$, $p > 0.05$).

nM (ref. 66)) have shown to exhibit antibacterial activity and cell proliferative behavior in the past.

This was expected as the GSNO solution made up only 5% v/v of the total NE, and the GSNO loaded into the ePTFE-20 and ePTFE-25 samples were between 40 and 60 μg cm^{-2} (Fig. 4A). Although a major limitation is the relatively low NO release, it is crucial to emphasize that the materials remain functional and effective within the first 4 h. This time frame is particularly significant in clinical settings, as the initial hours following device implantation play a critical role in determining the success of the procedure. During this period, the risk of complications such as thrombosis or bacterial adhesion pose a major concern,[67,68] making it essential for the implanted material to maintain its viability and performance. Therefore, even a modest NO release within this window can still contribute to improved biocompatibility, reduced immune response, and enhanced overall outcomes. Therefore, the NO release after 30 min of UV sterilization was also assessed. The ePTFE-20 and ePTFE-25 samples exhibited around 0.23 and 0.45 × 10^{-10} mol min^{-1} cm^{-2} of NO release, respectively, after sterilization (Fig. S8A). Although the NO released from ePTFE-20 was reduced from time 0 and 30 min (Fig. S8B), that level of NO was sustained for at least 4 h. The NO from ePTFE-25 did not significantly decrease after 30 min of UV sterilization, likely due to the higher amount of GSNO loaded into the NE (Fig. S8B).

With the GSNO solution encompassed in the NE and swelled in hydrophobic ePTFE, it is protected from any additional hydration and hydrolysis. The protective hydrophobic barriers also prevent excessive GSNO diffusion from the matrix, thereby preventing much NO release from diffused molecules. As described previously, the GSNO began degrading and releasing NO as soon as the GSNO solution in PBS w/ EDTA was prepared during the fabrication for all experiments. Therefore, despite the higher loading capacity of the 25 mg mL^{-1} GSNO solution incorporated into ePTFE-25, and without additional hydration to further catalyze NO release, both

ePTFE-20 and ePTFE-25 were diffusing GSNO and NO at the same rate (Fig. 5B). Due to the insignificant difference between ePTFE-20 and ePTFE-25 in terms of anti-fouling capability, GSNO loading and leaching, and NO release after 24 h, all further biological assessments were performed with ePTFE, ePTFE-NE, and ePTFE-20.
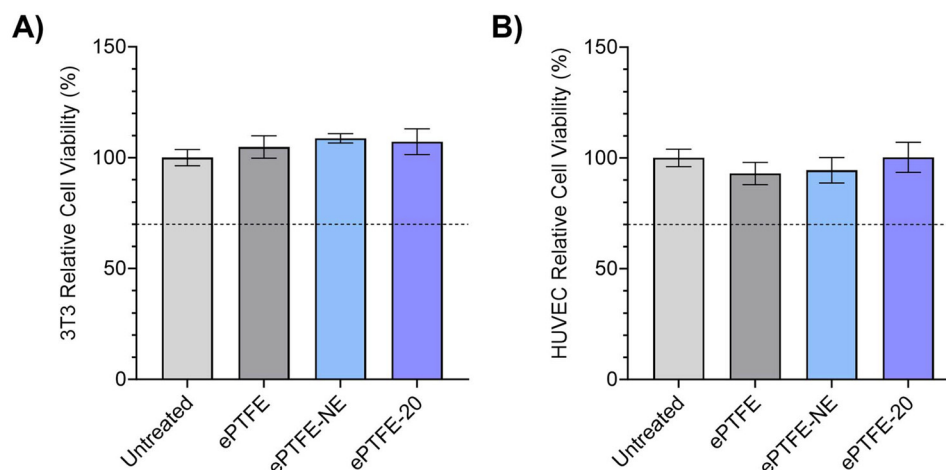
3.5. Biocompatibility assessment

3.5.1. Cytocompatibility. A key factor in the success and efficacy of indwelling medical devices are their inherent biocompatibility. Strictly speaking, the device and its constituents should not elicit excessive cell death in the surrounding environment. According to ISO 10993-5,[47] the threshold for relative cell viability to be considered cytocompatible and deemed suitable for biomedical applications is 70%. Therefore, NIH 3T3 mouse fibroblast cells and primary human umbilical vein endothelial cells (HUVEC) were cultured and indirectly exposed to the GSNO-NE infused ePTFE samples and their controls *via* leachate exposure. The viability of the cells was quantified with the colorimetric MTT assay.

After 24 h exposure to the sample leachates, the mouse fibroblast cells and HUVECs appeared to be visually unchanged (Fig. S9). Exposure to the MTT working solution revealed an abundance of formazan crystals across all of the sample types, indicating high viability. The mouse fibroblast cells and HUVECs demonstrated relative cell viability of greater than 95% for ePTFE, ePTFE-NE, and ePTFE-20 (Fig. 6A and B).

Commercial ePTFE has been previously used in blood-contacting devices such as vascular grafts, vascular stents, and sutures due to its innate hydrophobicity.[69,70] It is relatively cytocompatible in these applications alone,[71,72] but the addition of a NO donor and a NE makes for a more complex matrix. The liquid infusion of the NE into ePTFE did not significantly affect the viability of cells as the NE did not deplete from the surface or bulk material to suffocate the cells and result in cell death. In combination, the low NO release concentrations were near physiological levels,[65] allowing for the

Fig. 6 (A) Relative cell viability of 3T3 cells and (B) HUVECs when exposed to GSNO-NE-infused ePTFE and its controls. The dashed line at 70% cell viability represents the ISO threshold for cell cytocompatibility. The addition of the NE, and subsequently GSNO, into the ePTFE did not cause significant decrease in cell viability as the NO released was not high enough to elicit cytotoxic effects ($n = 4$, $p > 0.05$).

promotion of cell viability. The results directly translate to biomaterial suitability for medical devices.

3.5.2. Hemolytic evaluation. While mammalian cell viability is imperative for the efficacy and safety of a device, the hemocompatibility of a device must also be a paramount consideration. Thrombosis and embolisms are major causes of device failure,[73–75] potentially resulting in the removal and replacement of the device from the patient's body and an increased recovery period. Blood-contacting devices may be constantly exposed to blood; if hemolysis were to occur at the point of device contact, drastic ramifications and the initiation of the clotting cascade would render the device unusable. Therefore, the hemolytic activity of the ePTFE-20 samples was evaluated against its controls with porcine whole blood exposure. After 3 h incubating with the whole blood, the samples were removed, and the absorbance of the blood supernatant was read. All sample types exhibited a hemolytic index of <2% (Table 1). According to ISO 10993-4 standards,[48] hemolytic indices <2% do not indicate hemolytic activity, demonstrating the ePTFE-20's biocompatibility and ability to maintain homeostasis.

3.6. Prevention of protein adsorption

Implanted medical devices, especially blood-contacting medical devices, are prone to surface–protein interactions and

fouling in the presence of blood proteins. The clotting cascade is triggered when foreign materials, such as medical devices, are introduced into the body, leading to downstream tissue factors converting to their activated form and the conversion of fibrinogen to fibrin.[76] These conversions, specifically fibrinogen into fibrin, aid in thrombus formation, additionally allowing other blood components like platelets and blood cells to aggregate and clot.[76] Bacterial adhesion has been shown to increase with the aggregation of platelets, red blood cells, and proteins, which exacerbates infection and device failure around the thrombus site.[77] While NO has demonstrated excellent antibacterial and anti-platelet capabilities in recent decades, NO release tends to increase protein adsorption surfaces,[78] which in turn amplifies bacterial infection and platelet aggregation. Therefore, combination strategies must be employed to address protein fouling in NO-releasing materials.
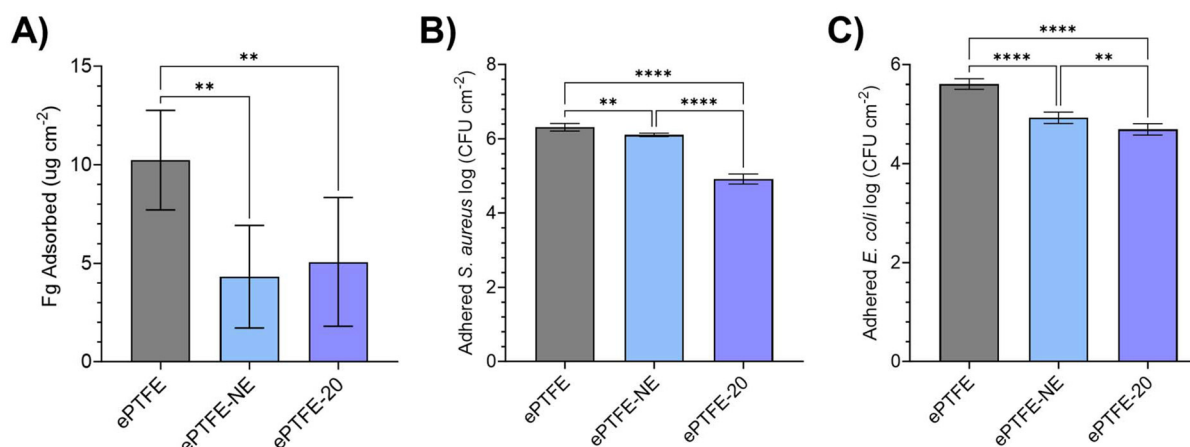
Fibrinogen (Fg) was used as the model protein in this study as it is a key protein in the clotting cascade. The samples were incubated with fluorescently labelled Fg (FITC-Fg); the non-adsorbed FITC-Fg was washed off of the samples. The adsorbed Fg was quantified on the samples. While the ePTFE control exhibited 10.23 ± 2.53 µg cm^{-2} of Fg adsorbed on the surface (Fig. 7A), both ePTFE-NE and ePTFE-20 demonstrated a 57.87% and 50.51% reduction of adsorbed Fg, respectively (Fig. S10).

As a highly hydrophobic and relatively cytocompatible material, ePTFE alone typically does not adsorb large quantities of fibrinogen, usually around 10 µg cm^{-2} or less.[79,80] The slippery NE modification introduced an especially hydrophobic and low surface tension environment that prevented fibrinogen from adsorbing on the surface. Recall that the surface tension of *n*-hexadecane is 27.47 mN m^{-1}. While lower than water, the surface tension of fibrongen in PBS (55 ± 2 mN m^{-1})[81] is greater than that of the NE; the lower surface tension NE can spread

Table 1 Hemolytic index (%) of ePTFE-20 compared to its controls. The inclusion of NO donor GSNO into the NE did not affect ePTFE's inherently hemocompatible nature. These results indicate that a negligible amount of red blood cells were lysed when exposed to the samples ($n = 6$, $p > 0.05$)

Sample	Hemolytic index (%)
ePTFE	0 ± 0.1876
ePTFE-NE	0 ± 0.1817
ePTFE-20	0 ± 0.2216

Fig. 7 (A) Fibrinogen adsorption on ePTFE-20 surface and its controls. After incubation with FITC-Fg, a reduction of Fg was demonstrated on ePTFE-NE and ePTFE-20 compared to control ePTFE, asserting that the presence of the slippery surface aided in preventing protein adsorption (n = 8, ***$p < 0.01$). (B) Reduction of bacterial adhesion of *S. aureus* and (C) *E. coli* on ePTFE-20 and its controls. Although the ePTFE-NE was able to reduce the number of adhered bacteria alone, the combination of the NO release and slippery surface (ePTFE-20) proved to significantly increase the antibacterial capacity of ePTFE (n = 6, ***$p < 0.01$, ****$p < 0.0001$).

and allow for the fibrinogen to slide off. Even though previous reports demonstrate higher Fg adsorption on NO-releasing substrates, the incorporation of GSNO in ePTFE-20 did not significantly increase the amount of Fg adsorbed compared to ePTFE or ePTFE-NE, further validating the need for combination strategies to combat protein fouling in NO-releasing materials.

3.7. Antibacterial performance

Nosocomial infections, while treatable, remain a prevalent complication associated with device implantation. Antibiotics are typically administered as a prophylactic measure to combat the onset of infection as well as treat existing infections. However, bacteria are trending towards antibiotic resistance;[82] antibiotics are becoming increasingly ineffective against bacteria due to their bulky molecular structure and inability to penetrate through biofilm extracellular polymeric substances (EPS).[83,84] It is especially paramount to prevent the onset of bacterial infection in the early hours immediately after surgical device implantation.[59,60] Once the bacteria mature into a dormant state within the biofilm, attacking them with antibiotics becomes nearly impossible. Therefore, other strategies such as bioactive agent release and passive anti-fouling mechanisms have come to the forefront of research. In the present work, the NO release and slippery surface of ePTFE-20 are employed as a dual-action strategy to prevent viable bacterial adhesion. The therapeutic levels of NO in combination with the low surface tension of the NE creates an environment that is not favorable for bacteria to thrive.

The combination of NO release and slippery NE-infused surfaces addresses the growing need for immediate prevention of bacterial infection upon implantation. While the control ePTFE did not demonstrate any bactericidal capabilities, the NO-releasing and slippery ePTFE-20 was able to significantly reduce the number of gram-positive *S. aureus* and gram-nega-

tive *E. coli* that adhered to the surface in a 4 h adhesion study by 95.94% and 87.81%, respectively, by both active and passive means compared to both the control and ePTFE-NE (Fig. 7B and C). Although the NO release from ePTFE-20 was on the lower end of the physiological range (between $0.25-0.36 \times 10^{-10}$ mol min^{-1} cm^{-2} for the duration of the experiment), the release was still enough to cause a broad-spectrum bactericidal effect on both *S. aureus* and *E. coli*, suggesting that these levels of NO release are sufficient for antibacterial function. This is due to the production of reactive nitrogen and oxide species with NO that led to bacterial lysis through altering DNA, inhibiting enzyme function, and lipid peroxidation,[85] as well as by acting as a cell signaler that can disrupt bacteria biofilms.[32,66] The ePTFE-20 was more effective against *S. aureus* than *E. coli* (Fig. S11), which is likely due to the difference in bacterial membrane composition. Gram-negative bacteria like *E. coli* have an additional protective peptidoglycan cell wall and lipopolysaccharide outer membrane,[86] which impedes NO's bactericidal mechanisms.[87,88] As gram-positive bacteria lack the protective outer membranes, they are more susceptible to NO's bactericidal capabilities. Concurrently, the slippery surface of the material physically prevented bacteria from adhering and fouling the material surface. At these same concentrations of NO, the NO induces mammalian cell proliferation by enhancing different growth factors and enzymatic activity.[89] Only when the NO concentration reaches ~1 µM does the nitrosation of critical proteins on mammalian cells occur and begin to inhibit cell function.[89]

While the ePTFE-NE was able to significantly reduce the adhesion of both *S. aureus* and *E. coli*, it had an opposite effect compared to ePTFE-20 in that the ePTFE-NE reduced *E. coli* adhesion more than *S. aureus*. The nanoemulsion's bulk phase is composed of *n*-hexadecane, and the chemistry/physics of a hydrocarbon lubricant can influence species-specific attach-

ment. *n*-hexadecane forms a hydrophobic liquid barrier that effectively blocks motility- and pili/flagella-mediated trapping, which disproportionately suppresses initial attachment of motile gram-negative bacteria such as *E. coli*.[90] By contrast, the surface of *S. aureus* are relatively hydrophobic and express protein adhesins (Microbial Surface Components Recognizing Adhesive Matrix Molecules – MSCRAMMs)[91] that can potentially bind to the oil–water interface itself. Consequently, the *S. aureus* was less sensitive to the low-friction effect of a *n*-hexadecane SNIPS in short assays. The results suggest that *n*-hexadecane-based SNIPS strongly reduces initial *E. coli* attachment while producing a smaller short-term effect on *S. aureus*.

This work demonstrates that ePTFE-20 performs relatively well against *S. aureus* with reduced efficacy against *E. coli* when compared to previous works that observe either low NO release with PTFE coatings[92] or 4 h bacterial adhesion studies.[93] Chug *et al.* recently reported a significant reduction of *S. aureus* and *E. coli* adhesion (99.45% and 99.36%, respectively) when exposed to NO release catalyzed by light in a 4 h adhesion study.[93] The release from the ePTFE-20 performed comparably against *S. aureus*; however, ePTFE-20 did not exhibit as much reduction of *E. coli*. This is most likely attributed to the lack of light catalysis in this present work. The added light catalysis in the aforementioned study allowed more NO to be released from the material, which aided in antibacterial behavior. In a 24 h bacterial adhesion study, Mondal *et al.* exposed NO-releasing samples coated PTFE particles and observed a 99.3% and 99.1% reduction of *S. aureus* and *E. coli*.[92] Here, the better performance of bacterial reduction is attributed to the higher initial NO release within the first 24 h. As ePTFE-20 had an initial NO release around 0.4×10^{-10} mol min^{-1} cm^{-2}, it had an immediate disadvantage compared to the previous report. Despite the limitations of ePTFE-20, the NO released from ePTFE-20 was enough to provide a significant reduction of bacteria compared to control ePTFE and ePTFE-NE. It is the most effective in the immediate hours after infection, but continuous replenishment from the slippery NE further prevents bacterial adhesion when the NO supply has been depleted.

4. Conclusions

Techniques to prevent bacterial infection and thrombosis have become a prevalent concern among healthcare researchers in the last decade. While antibiotics and anticoagulants are still administered and are effective to an extent, the rise of antibiotic resistance and adverse effects of anticoagulants continuously concern healthcare professionals. Without alternatives to circumvent antibiotic resistance and the adverse effects of anticoagulants, patients face ineffective treatments, longer recovery times, and potentially more costly expenses.

This work introduced a slippery, NO-releasing platform that allows for a hydrophilic and water-soluble therapeutic to be loaded into a hydrophobic substrate through the incorporation of the NO donor GSNO into an *n*-hexadecane-based nanoemul-

sion. The combination material ePTFE-20 demonstrated antifouling behavior quantified by sliding angle measurements below 20°, as well as physiological levels of NO release for 24 h. Neither the ePTFE-20 material nor any of its constituents exhibited cytotoxic tendencies towards mammalian mouse fibroblast cells and HUVECs while also significantly reducing the number of adhered *S. aureus* and *E. coli* during the critical period of infection onset. In addition to the ePTFE-20's cytocompatibility, the material remained non-hemolytic with negligible red blood cell lysis and a hemolytic index of less than 2%. Overall, the NO-releasing slippery nanoemulsion platform holds potential for future biomedical applications.

Conflicts of interest

The authors declare the following competing financial interest (s): Elizabeth J. Brisbois is cofounder and maintains a financial interest in a startup company investigating nitric oxide as a biomedical therapeutic for medical devices.

Author contributions

Grace H. Nguyen: conceptualization, data curation, formal analysis, investigation, methodology, validation, visualization, writing – original draft, writing – review & editing. Aasma Sapkota: formal analysis, investigation, methodology, validation, visualization, writing – review & editing. Elizabeth J. Brisbois: project administration, data curation, funding acquisition, resources, supervision, writing – review & editing.

Data availability

Data will be made available upon a reasonable request.

Supplementary information is available. See DOI: **https://doi.org/10.1039/d5bm00900f**.

Acknowledgements

References

1 Centers for Disease Control and Prevention, *HAIs: Reports and Data*, 2024.

2 Centers for Disease Control and Prevention, *Data and Statistics on Venous Thromboembolism*, 2024.

3 J. S. Vanepps and J. G. Younger, Implantable Device-Related Infection, *Shock*, 2016, **46**(6), 597–608, DOI: **10.1097/shk.0000000000000692**.

4   I. H. Jaffer, J. C. Fredenburgh, J. Hirsh and J. I. Weitz, Medical device–induced thrombosis: what causes it and how can we prevent it?, *J. Thromb. Haemostasis*, 2015, **13**, S72–S81, DOI: **10.1111/jth.12961**.

5   D. Bluestein, S. Einav and M. J. Slepian, Device thrombogenicity emulation: A novel methodology for optimizing the thromboresistance of cardiovascular devices, *J. Biomech.*, 2013, **46**(2), 338–344, DOI: **10.1016/j.jbiomech.2012.11.033**.

6   E. G. Butchart, A. Ionescu, N. Payne, J. Giddings, G. L. Grunkemeier and A. G. Fraser, A New Scoring System to Determine Thromboembolic Risk After Heart Valve Replacement, *Circulation*, 2003, **108**, II-68–II-74, DOI: **10.1161/01.cir.0000087383.62522.1e**.

7   E. G. Butchart, H.-H. Li, N. Payne, K. Buchan and G. L. Grunkemeier, Twenty years' experience with the Medtronic Hall valve, *J. Thorac. Cardiovasc. Surg.*, 2001, **121**(6), 1090–1100, DOI: **10.1067/mtc.2001.113754**.

8   P. W. Stone, Economic burden of healthcare-associated infections: an American perspective, *Expert Rev. Pharmacoecon. Outcomes Res.*, 2009, **9**(5), 417–422, DOI: **10.1586/erp.09.53**.

9   K. Gidey, M. T. Gidey, B. Y. Hailu, Z. B. Gebreamlak and Y. L. Niriayo, Clinical and economic burden of healthcare-associated infections: A prospective cohort study, *PLoS One*, 2023, **18**(2), e0282141, DOI: **10.1371/journal.pone.0282141**.

10 G. Mancuso, A. Midiri, E. Gerace and C. Biondo, Bacterial Antibiotic Resistance: The Most Critical Pathogens, *Pathogens*, 2021, **10**(10), 1310, DOI: **10.3390/pathogens10101310**.

11 J. D. Bryers, Medical biofilms, *Biotechnol. Bioeng.*, 2008, **100**(1), 1–18, DOI: **10.1002/bit.21838**.

12 P. S. Stewart and J. William Costerton, Antibiotic, resistance of bacteria in biofilms, *Lancet*, 2001, **358**(9276), 135–138, DOI: **10.1016/s0140-6736(01)05321-1**.

13 S. Alban, Adverse Effects of Heparin, in *Heparin - A Century of Progress*, ed. R. Lever, B. Mulloy and C. P. Page, Springer Berlin Heidelberg, 2012, pp. 211–263.

14 M. D. Freedman, Oral Anticoagulants: Pharmacodynamics, Clinical Indications and Adverse Effects, *J. Clin. Pharmacol.*, 1992, **32**(3), 196–209, DOI: **10.1002/j.1552-4604.1992.tb03827.x**.

15 M. D. Freedman, Pharmacodynamics, Clinical Indications, and, Adverse Effects of Heparin, *J. Clin. Pharmacol.*, 1992, **32**(7), 584–596, DOI: **10.1002/j.1552-4604.1992.tb05765.x**.

16 E. J. Brisbois, M. Kim, X. Wang, A. Mohammed, T. C. Major, J. Wu, J. Brownstein, C. Xi, H. Handa, R. H. Bartlett, *et al.*, Improved Hemocompatibility of Multilumen Catheters via Nitric Oxide (NO) Release from S-Nitroso-N-acetylpenicillamine (SNAP) Composite Filled Lumen, *ACS Appl. Mater. Interfaces*, 2016, **8**(43), 29270–29279, DOI: **10.1021/acsami.6b08707**.

17 M. J. Goudie, J. Pant and H. Handa, Liquid-infused nitric oxide-releasing (LINORel) silicone for decreased fouling, thrombosis, and infection of medical devices, *Sci. Rep.*, 2017, **7**, 13623, DOI: **10.1038/s41598-017-14012-9**.

18 L. Griffin, M. Douglass, M. Goudie, S. P. Hopkins, C. Schmiedt and H. Handa, Improved Polymer Hemocompatibility for Blood-Contacting Applications via S-Nitrosoglutathione Impregnation, *ACS Appl. Mater. Interfaces*, 2022, **14**(9), 11116–11123, DOI: **10.1021/acsami.1c24557**.

19 S. P. Hopkins, J. Pant, M. J. Goudie, C. Schmiedt and H. Handa, Achieving Long-Term Biocompatible Silicone via Covalently Immobilized S-Nitroso-N-acetylpenicillamine (SNAP) That Exhibits 4 Months of Sustained Nitric Oxide Release, *ACS Appl. Mater. Interfaces*, 2018, **10**(32), 27316–27325, DOI: **10.1021/acsami.8b08647**.

20 A. Mondal, M. Douglass, S. P. Hopkins, P. Singha, M. Tran, H. Handa and E. J. Brisbois, Multifunctional S-Nitroso-N-acetylpenicillamine-Incorporated Medical-Grade Polymer with Selenium Interface for Biomedical Applications, *ACS Appl. Mater. Interfaces*, 2019, **11**(38), 34652–34662, DOI: **10.1021/acsami.9b10610**.

21 A. Sapkota, A. Mondal, M. K. Chug and E. J. Brisbois, Biomimetic catheter surface with dual action NO-releasing and generating properties for enhanced antimicrobial efficacy, *J. Biomed. Mater. Res., Part A*, 2023, **111**(10), 1627–1641, DOI: **10.1002/jbm.a.37560**.

22 R. Kumar, H. Massoumi, M. K. Chug and E. J. Brisbois, S-Nitroso-N-acetyl-l-cysteine, Ethyl Ester (SNACET) Catheter Lock Solution to Reduce Catheter-Associated Infections, *ACS Appl. Mater. Interfaces*, 2021, **13**(22), 25813–25824, DOI: **10.1021/acsami.1c06427**.

23 M. K. Chug, C. Feit and E. J. Brisbois, Increasing the Lifetime of Insulin Cannula with Antifouling and Nitric Oxide Releasing Properties, *ACS Appl. Bio Mater.*, 2019, **2**(12), 5965–5975, DOI: **10.1021/acsabm.9b00908**.

24 N. M. L. Hansen, K. Jankova and S. Hvilsted, Fluoropolymer materials and architectures prepared by controlled radical polymerizations, *Eur. Polym. J.*, 2007, **43**(2), 255–293, DOI: **10.1016/j.eurpolymj.2006.11.016**.

25 R. Koguchi, K. Jankova, Y. Tanaka, A. Yamamoto, D. Murakami, Q. Yang, B. Ameduri and M. Tanaka, Altering the bio-inert properties of surfaces by fluorinated copolymers of mPEGMA, *Biomater. Adv.*, 2023, **153**, 213573, DOI: **10.1016/j.bioadv.2023.213573**.

26 M. Renfrew and E. Lewis, Polytetrafluoroethylene. Heat resistant, chemically inert plastic, *Ind. Eng. Chem.*, 1946, **38**(9), 870–877.

27 G. Zapsas, Y. Patil, Y. Gnanou, B. Ameduri and N. Hadjichristidis, Poly(vinylidene fluoride)-based complex macromolecular architectures: From synthesis to properties and applications, *Prog. Polym. Sci.*, 2020, **104**, 101231, DOI: **10.1016/j.progpolymsci.2020.101231**.

28 K. A. Broniowska, A. R. Diers and N. Hogg, S-Nitrosoglutathione., *Biochim. Biophys. Acta, Gen. Subj.*, 2013, **1830**(5), 3173–3181, DOI: **10.1016/j.bbagen.2013.02.004**.

29 M. G. de Oliveira, S. M. Shishido, A. B. Seabra and N. H. Morgon, Thermal Stability of Primary S-Nitrosothiols: Roles of Autocatalysis and Structural Effects on the Rate of

Nitric Oxide Release, *J. Phys. Chem. A*, 2002, **106**(38), 8963–8970, DOI: **10.1021/jp025756u**.

30   A. B. Seabra and M. G. de Oliveira, Poly(vinyl alcohol) and poly(vinyl pyrrolidone) blended films for local nitric oxide release, *Biomaterials*, 2004, **25**(17), 3773–3782, DOI: **10.1016/j.biomaterials.2003.10.035**.

31   L. M. Estes Bright, M. R. S. Garren, M. Ashcraft, A. Kumar, H. Husain, E. J. Brisbois and H. Handa, Dual Action Nitric Oxide and Fluoride Ion-Releasing Hydrogels for Combating Dental Caries, *ACS Appl. Mater. Interfaces*, 2022, **14**(19), 21916–21930, DOI: **10.1021/acsami.2c02301**.

32   L. M. Estes Bright, L. Griffin, A. Mondal, S. Hopkins, E. Ozkan and H. Handa, Biomimetic gasotransmitter-releasing alginate beads for biocompatible antimicrobial therapy, *J. Colloid Interface Sci.*, 2022, **628**, 911–921, DOI: **10.1016/j.jcis.2022.08.113**.

33   W. J. Brittain and S. Minko, A structural definition of polymer brushes, *J. Polym. Sci., Part A: Polym. Chem.*, 2007, **45**(16), 3505–3512, DOI: **10.1002/pola.22180**.

34   L. Hao, R. Jiang, J. Gao, J. Xu, L.-N. Tian, X. Zhang, S. Zhou, J. Zhao and L. Ren, Metal-organic framework (MOF)-based slippery liquid-infused porous surface (SLIPS) for purely physical antibacterial applications, *Appl. Mater. Today*, 2022, **27**, 101430, DOI: **10.1016/j.apmt.2022.101430**.

35   A. Jaggessar, H. Shahali, A. Mathew and P. K. D. V. Yarlagadda, Bio-mimicking nano and micro-structured surface fabrication for antibacterial properties in medical implants, *J. Nanobiotechnol.*, 2017, **15**, 64, DOI: **10.1186/s12951-017-0306-1**.

36   X. Meng, Z. Wang, L. Wang, L. Heng and L. Jiang, A stable solid slippery surface with thermally assisted self-healing ability, *J. Mater. Chem. A*, 2018, **6**(34), 16355–16360, DOI: **10.1039/c8ta05886e**.

37   F. Pan, S. Zhang, S. Altenried, F. Zuber, Q. Chen and Q. Ren, Advanced antifouling and antibacterial hydrogels enabled by controlled thermo-responses of a biocompatible polymer composite, *Biomater. Sci.*, 2022, **10**(21), 6146–6159, DOI: **10.1039/d2bm01244h**.

38   E. Prudnikov, I. Polishchuk, A. Sand, H. A. Hamad, N. Massad-Ivanir, E. Segal and B. Pokroy, Self-assembled fatty acid crystalline coatings display superhydrophobic antimicrobial properties, *Mater. Today Bio*, 2023, **18**, 100516, DOI: **10.1016/j.mtbio.2022.100516**.

39   T.-S. Wong, S. H. Kang, S. K. Y. Tang, E. J. Smythe, B. D. Hatton, A. Grinthal and J. Aizenberg, Bioinspired self-repairing slippery surfaces with pressure-stable omniphobicity, *Nature*, 2011, **477**(7365), 443–447, DOI: **10.1038/nature10447**.

40   M. A. Samaha and M. Gad-El-Hak, Slippery surfaces: A decade of progress, *Phys. Fluids*, 2021, **33**(7), 071301, DOI: **10.1063/5.0056967**.

41   M. Villegas, Y. Zhang, N. Abu Jarad, L. Soleymani and T. F. Didar, Liquid-Infused Surfaces: A Review of Theory, Design, and Applications, *ACS Nano*, 2019, **13**(8), 8517–8536, DOI: **10.1021/acsnano.9b04129**.

42   H. Li, M. Yan and W. Zhao, Designing a MOF-based slippery lubricant-infused porous surface with dual functional anti-fouling strategy, *J. Colloid Interface Sci.*, 2022, **607**, 1424–1435, DOI: **10.1016/j.jcis.2021.09.052**.

43   H. Agarwal, T. J. Polaske, G. Sánchez-Velázquez, H. E. Blackwell and D. M. Lynn, Slippery nanoemulsion-infused porous surfaces (SNIPS): anti-fouling coatings that can host and sustain the release of water-soluble agents, *Chem. Commun.*, 2021, **57**(12691–12694), DOI: **10.1039/d1cc04645d**.

44   A. Gupta, H. B. Eral, T. A. Hatton and P. S. Doyle, Nanoemulsions: formation, properties and applications, *Soft Matter*, 2016, **12**(11), 2826–2841, DOI: **10.1039/c5sm02958a**.

45   T. G. Mason, J. N. Wilking, K. Meleson, C. B. Chang and S. M. Graves, Nanoemulsions: formation, structure, and physical properties, *J. Phys.: Condens. Matter*, 2006, **19**, 079001, DOI: **10.1088/0953-8984/19/7/079001**.

46   T. W. Hart, Some observations concerning the S-nitroso and S-phenylsulphonyl derivatives of L-cysteine and gluta-thione, *Tetrahedron Lett.*, 1985, **26**(16), 2013–2016, DOI: **10.1016/S0040-4039(00)98368-0**.

47   International Organization for Standardization, *ISO 10993-5: 2009 Biological evaluation of medical devices - Part 5: Test for in vitro cytotoxicity*, 2009.

48   International Organization for Standardization. *ISO 10993-4: 2017 Biological evaluation of medical devices—Part 4: Selection of tests for interactions with blood*, International Organizational for Standardization Geneve, 2017.

49   M. Ashcraft, M. Douglass, M. Garren, A. Mondal, L. E. Bright, Y. Wu and H. Handa, Nitric Oxide-Releasing Lock Solution for the Prevention of Catheter-Related Infection and Thrombosis, *ACS Appl. Bio Mater.*, 2022, **5**(4), 1519–1527, DOI: **10.1021/acsabm.1c01272**.

50   W. I. Goldburg, Dynamic light scattering, *Am. J. Phys.*, 1999, **67**(12), 1152–1160, DOI: **10.1119/1.19101**.

51   P. A. Hassan, S. Rana and G. Verma, Making Sense of Brownian Motion: Colloid Characterization by Dynamic Light Scattering, *Langmuir*, 2015, **31**(1), 3–12, DOI: **10.1021/la501789z**.

52   Y. Zhou, Q. Zhang, J. Wu, C. Xi and M. E. Meyerhoff, Synthesis and Characterization of a Fluorinated S-Nitrosothiol as the Nitric Oxide Donor for Fluoropolymer-Based Biomedical Device Applications, *J. Mater. Chem. B*, 2018, **6**(38), 6142–6152, DOI: **10.1039/c8tb01814f**.

53   Y. Zhou, J. Tan, Y. Dai, Y. Yu, Q. Zhang and M. E. Meyerhoff, Synthesis and nitric oxide releasing properties of novel fluoroS-nitrosothiols, *Chem. Commun.*, 2019, **55**(3), 401–404, DOI: **10.1039/c8cc08868c**.

54   Y. Zhou, J. Tan, J. Wu, Q. Zhang, J. Andre, C. Xi, Z. Chen and M. E. Meyerhoff, Nitric oxide releasing poly(vinylidene fluoride-co-hexafluoropropylene) films using a fluorinated nitric oxide donor to greatly decrease chemical leaching, *Acta Biomater.*, 2019, **90**, 112–121, DOI: **10.1016/j.actbio.2019.04.021**.

55   G. H. Nguyen, M. Garren, Y. Wu, A. Mondal, H. Handa and E. J. Brisbois, Multifunctional slippery nanoemulsion-infused porous nitric oxide-releasing surfaces, *J. Colloid Interface Sci.*, 2025, **689**, 137199, DOI: **10.1016/j.jcis.2025.02.207**.

56 H. S. Kato, M. Kawai, K. Akagi and S. Tsuneyuki, Interaction of condensed water molecules with hydroxyl and hydrogen groups on Si(001), *Surf. Sci.*, 2005, **587**(1), 34–40, DOI: 10.1016/j.susc.2005.04.032.

57 J. J. Jasper, The Surface Tension of Pure Liquid Compounds, *J. Phys. Chem. Ref. Data*, 1972, **1**(4), 841–1010, DOI: 10.1063/1.3253106.

58 L. I. Rolo, A. I. Caço, A. J. Queimada, I. M. Marrucho and J. A. P. Coutinho, Surface Tension of Heptane, Decane, Hexadecane, Eicosane, and Some of Their Binary Mixtures, *J. Chem. Eng. Data*, 2002, **47**(6), 1442–1445, DOI: 10.1021/je025536+.

59 M. Gamil and A. Fanning, The first 24 hours after surgery, *Anaesthesia*, 1991, **46**(9), 712–715, DOI: 10.1111/j.1365-2044.1991.tb09761.x.

60 D. C. Classen, R. S. Evans, S. L. Pestotnik, S. D. Horn, R. L. Menlove and J. P. Burke, The Timing of Prophylactic Administration of Antibiotics and the Risk of Surgical-Wound Infection, *N. Engl. J. Med.*, 1992, **326**(5), 281–286, DOI: 10.1056/NEJM199201303260501.

61 Y. Qian, M. K. Chug and E. J. Brisbois, Nitric Oxide-Releasing Silicone Oil with Tunable Payload for Antibacterial Applications, *ACS Appl. Bio Mater.*, 2022, **5**(7), 3396–3404, DOI: 10.1021/acsabm.2c00358.

62 R. Devine, M. J. Goudie, P. Singha, C. Schmiedt, M. Douglass, E. J. Brisbois and H. Handa, Mimicking the Endothelium: Dual Action Heparinized Nitric Oxide Releasing Surface, *ACS Appl. Mater. Interfaces*, 2020, **12**(18), 20158–20171, DOI: 10.1021/acsami.9b22277.

63 M. E. Douglass, M. J. Goudie, J. Pant, P. Singha, S. Hopkins, R. Devine, C. W. Schmiedt and H. Handa, Catalyzed Nitric Oxide Release via Cu Nanoparticles Leads to an Increase in Antimicrobial Effects and Hemocompatibility for Short-Term Extracorporeal Circulation, *ACS Appl. Bio Mater.*, 2019, **2**(6), 2539–2548, DOI: 10.1021/acsabm.9b00237.

64 L. M. Estes Bright, M. R. S. Garren, M. Douglass and H. Handa, Synthesis and Characterization of Nitric Oxide-Releasing Ampicillin as a Potential Strategy for Combatting Bacterial Biofilm Formation, *ACS Appl. Mater. Interfaces*, 2023, **15**(12), 15185–15194, DOI: 10.1021/acsami.3c00140.

65 M. W. Vaughn, L. Kuo and J. C. Liao, Estimation of nitric oxide production and reactionrates in tissue by use of a mathematical model, *Am. J. Physiol.: Heart Circ. Physiol.*, 1998, **274**(6), H2163–H2176, DOI: 10.1152/ajpheart.1998.274.6.H2163.

66 N. Barraud, D. J. Hassett, S.-H. Hwang, S. A. Rice, S. Kjelleberg and J. S. Webb, Involvement of Nitric Oxide in Biofilm Dispersal of *Pseudomonas aeruginosa*, *J. Bacteriol.*, 2006, **188**(21), 7344–7353, DOI: 10.1128/jb.00779-06.

67 M. Zabaglo, S. W. Leslie, T. Sharman, *Postoperative Wound Infections*, StatPearls Publishing, StatPearls, 2024.

68 V. Khalameizer, Multiple-vein thrombosis and pulmonary embolism after pacemaker implantation treated by thrombolysis, *Europace*, 2004, **6**(5), 453–456, DOI: 10.1016/j.eupc.2004.05.005.

69 C. Sperati, in *High Performance Polymers: Their Origin and Development*, ed. R. B Seymour and G. S Kirshenbaum, Elsevier Science Publishing, New York, Amsterdam, London, 1986.

70 A. I. Cassady, N. M. Hidzir and L. Grøndahl, Enhancing expanded poly(tetrafluoroethylene) (ePTFE) for biomaterials applications, *J. Appl. Polym. Sci.*, 2014, **131**(15), 40533, DOI: 10.1002/app.40533.

71 P. C. S. Bota, A. M. B. Collie, P. Puolakkainen, R. B. Vernon, E. H. Sage, B. D. Ratner and P. S. Stayton, Biomaterial topography alters healing in vivo and monocyte/macrophage activation in vitro, *J. Biomed. Mater. Res., Part A*, 2010, **95A**(2), 649–657, DOI: 10.1002/jbm.a.32893.

72 R. Y. Kannan, H. J. Salacinski, P. E. Butler, G. Hamilton and A. M. Seifalian, Current status of prosthetic bypass grafts: A review, *J. Biomed. Mater. Res., Part B*, 2005, **74B**(1), 570–581, DOI: 10.1002/jbm.b.30247.

73 T. Hilal, J. Mudd and T. G. DeLoughery, Hemostatic complications associated with ventricular assist devices, *Res. Pract. Thromb. Haemostasis*, 2019, **3**(4), 589–598, DOI: 10.1002/rth2.12226.

74 A. V. Finn, M. Joner, G. Nakazawa, F. Kolodgie, J. Newell, M. C. John, H. K. Gold and R. Virmani, Pathological Correlates of Late Drug-Eluting Stent Thrombosis, *Circulation*, 2007, **115**(18), 2435–2441, DOI: 10.1161/CIRCULATIONAHA.107.693739.

75 P. Qi, M. F. Maitz and N. Huang, Surface modification of cardiovascular materials and implants, *Surf. Coat. Technol.*, 2013, **233**, 80–90, DOI: 10.1016/j.surfcoat.2013.02.008.

76 S. Palta, R. Saroa and A. Palta, Overview of the coagulation system, *Indian J. Anaesth.*, 2014, **58**(5), 515–523, DOI: 10.4103/0019-5049.144643.

77 G. W. Charville, E. M. Hetrick, C. B. Geer and M. H. Schoenfisch, Reduced bacterial adhesion to fibrinogen-coated substrates via nitric oxide release, *Biomaterials*, 2008, **29**(30), 4039–4044, DOI: 10.1016/j.biomaterials.2008.07.005.

78 S. M. Lantvit, B. J. Barrett and M. M. Reynolds, Nitric oxide releasing material adsorbs more fibrinogen, *J. Biomed. Mater. Res., Part A*, 2013, **101**(11), 3201–3210, DOI: 10.1002/jbm.a.34627.

79 Y. J. Choi, S. K. Choung, C. M. Hong, I. S. Shin, S. N. Park, S. H. Hong, H. K. Park, Y. H. Park, Y. Son and I. Noh, Evaluations of blood compatibility via protein adsorption treatment of the vascular scaffold surfaces fabricated with polylactide and surface–modified expanded polytetrafluoroethylene for tissue engineering applications, *J. Biomed. Mater. Res., Part A*, 2005, **75A**(4), 824–831, DOI: 10.1002/jbm.a.30468.

80 T. Goyama, Y. Fujii, G. Muraoka, T. Nakatani, D. Ousaka, Y. Imai, N. Kuwada, T. Tsuji, T. Shuku, H. A. Uchida, *et al.*, Comprehensive hemocompatibility analysis on the application of diamond-like carbon to ePTFE artificial vascular prosthesis, *Sci. Rep.*, 2023, **13**(1), DOI: 10.1038/s41598-023-35594-7.

81 E. M. Hernández and E. I. Franses, Adsorption and surface tension of fibrinogen at the air/water interface, *Colloids*

Surf., A, 2003, **214**(1), 249–262, DOI: **10.1016/S0927-7757(02)00403-X**.

82 C. L. Ventola, The antibiotic resistance crisis: part 1: causes and threats, P T, 2015, **40**(4), 277–283.

83 W. Zhao, J. You, S. Yin, H. Yang, S. He, L. Feng, J. Li, Q. Zhao and L. Wei, Extracellular polymeric substances-antibiotics interaction in activated sludge: A review, Environ. Sci. Ecotechnol, 2023, **13**, 100212, DOI: **10.1016/j.ese.2022.100212**.

84 S. Li, G. Duan, Y. Xi, Y. Chu, F. Li and S.-H. Ho, Insights into the role of extracellular polymeric substances (EPS) in the spread of antibiotic resistance genes, Environ. Pollut., 2024, **343**, 123285, DOI: **10.1016/j.envpol.2023.123285**.

85 D. O. Schairer, J. S. Chouake, J. D. Nosanchuk and A. J. Friedman, The potential of nitric oxide releasing therapies as antimicrobial agents, Virulence, 2012, **3**(3), 271–279, DOI: **10.4161/viru.20328**.

86 T. J. Silhavy, D. Kahne and S. Walker, The Bacterial Cell Envelope, Cold Spring Harbor Perspect. Biol., 2010, **2**(5), a000414–a000414, DOI: **10.1101/cshperspect.a000414**.

87 A. Friedman, K. Blecher, D. Sanchez, C. Tuckman-Vernon, P. Gialanella, J. M. Friedman, L. R. Martinez and J. D. Nosanchuk, Susceptibility of Gram-positive and -negative bacteria to novel nitric oxide-releasing nanoparticle technology, Virulence, 2011, **2**(3), 217–221, DOI: **10.4161/viru.2.3.16161**.

88 M. Ashcraft, M. Garren, O. Lautner-Csorba, V. Pinon, Y. Wu, D. Crowley, J. Hill, Y. Morales, R. Bartlett, E. J. Brisbois, et al., Surface Engineering for Endothelium-Mimicking Functions to Combat Infection and Thrombosis in Extracorporeal Life Support Technologies, Adv. Healthcare Mater., 2024, **13**(22), 2400492, DOI: **10.1002/adhm.202400492**.

89 D. D. Thomas, L. A. Ridnour, J. S. Isenberg, W. Flores-Santana, C. H. Switzer, S. Donzelli, P. Hussain, C. Vecoli, N. Paolocci, S. Ambs, et al., The chemical biology of nitric oxide: Implications in cellular signaling, Free Radicals Biol. Med., 2008, **45**(1), 18–31, DOI: **10.1016/j.freeradbiomed.2008.03.020**.

90 A. K. Epstein, T. S. Wong, R. A. Belisle, E. M. Boggs and J. Aizenberg, Liquid-infused structured surfaces with exceptional anti-biofouling performance, Proc. Natl. Acad. Sci. U. S. A., 2012, **109**(33), 13182–13187, DOI: **10.1073/pnas.1201973109**.

91 T. J. Foster, J. A. Geoghegan, V. K. Ganesh and M. Höök, Adhesion, invasion and evasion: the many functions of the surface proteins of Staphylococcus aureus, Nat. Rev. Microbiol., 2014, **12**(1), 49–62, DOI: **10.1038/nrmicro3161**.

92 A. Mondal, R. Devine, L. Estes, J. Manuel, P. Singha, J. Mancha, M. Palmer and H. Handa, Highly hydrophobic polytetrafluoroethylene particle immobilization via polydopamine anchor layer on nitric oxide releasing polymer for biomedical applications, J. Colloid Interface Sci., 2021, **585**, 716–728, DOI: **10.1016/j.jcis.2020.10.051**.

93 M. K. Chug and E. J. Brisbois, Smartphone compatible nitric oxide releasing insert to prevent catheter-associated infections, J. Controlled Release, 2022, **349**, 227–240, DOI: **10.1016/j.jconrel.2022.06.043**.